Available online at www.sciencedirect.com
ScienceDirect
Journal of Nuclear Materials 363–365 (2007) 216–221
journal of nuclear materials
www.elsevier.com/locate/jnucmat

Transport of dust particles in tokamak devices

A.Yu. Pigarov [a,*], R.D. Smirnov [a], S.I. Krasheninnikov [a], T.D. Rognlien [b], M. Rosenberg [a], T.K. Soboleva [c]

[a] University of California at San Diego, La Jolla, CA, USA
[b] Lawrence Livermore National Laboratory, Livermore, CA, USA
[c] UNAM, Mexico, DistritoFederal, Mexico

Abstract

Recent advances in the dust transport modeling in tokamak devices are discussed. Topics include: (1) physical model for dust transport; (2) modeling results on dynamics of dust particles in plasma; (3) conditions necessary for particle growth in plasma; (4) dust spreading over the tokamak; (5) density profiles for dust particles and impurity atoms associated with dust ablation in tokamak plasma; and (6) roles of dust in material/tritium migration.

PACS: 52.55.Fa; 52.40.Hf; 52.25.Vy; 53.65.Pp

Keywords: Dust; Edge plasma; Impurity transport; UEDGE; DUSTT

1. Introduction

Dust has been identified as having a potentially large impact on fusion-scale plasma experiments [1–3]. Understanding and predicting the role of dust require models of the mechanisms of production, plasma and surface interactions, and transport within and outside the plasma. Furthermore, one must understand dust removal, as well as assessing dust impact on core plasma performance, tritium retention and in-vessel inventory, and the safety of next-step fusion devices. Indeed, dust safety limits and control are important parts of the ITER R&D program [1,2], including the development and validation of simulation capabilities. In the paper, we discuss modeling of dust transport in tokamaks, analyze the conditions leading to dust growth in plasma, study the penetrability of dust particles originating from the tokamak chamber through vacuum ducts, and present the results obtained with DUSTT and UEDGE codes on dust transport, dust particle density profiles, and density of impurities originated from dust ablation.

2. The DUSTT code

A physical model [3,4] for dust transport in fusion devices includes the dynamics of dust–plasma, dust–turbulence, and dust–surface interactions. The dynamics is strongly coupled to heating, charging, erosion, evaporation, and thermo-chemical

* Corresponding author.
E-mail address: apigarov@uscd.edu (A.Yu. Pigarov).

0022-3115/$ - see front matter © 2007 Elsevier B.V. All rights reserved.
doi:10.1016/j.jnucmat.2007.01.053

properties of dust particles. These processes have been incorporated into the DUST transport (DUSTT) code [4] that includes the following capabilities: a 2D curvilinear non-uniform mesh based on MHD equilibrium; multi-species plasma and neutral-gas parameters calculated by the edge plasma/neutrals transport code UEDGE; and tracking of test dust particles in 3D using the resulting force ($\boldsymbol{F}_{\rm tot}$, the vector sum of electric, ion and neutral friction, and gravity forces), particle and energy fluxes, and other parameters based on UEDGE data. DUSTT employs a Monte Carlo method to simulate collisions and to perform averaging over an ensemble of test dust particles.

In modeling, we assume that the dust particle is spherical with radius $R_{\rm d}$ and has uniform temperature $T_{\rm d}$. It is comprised of uniform solid matter with atom density $\rho_{\rm d}$, mass $m_{\rm d}$, heat capacity $C_{\rm d}(T_{\rm d})$; so dust mass is $M_{\rm d} = 4\pi R_{\rm d}^3 \rho_{\rm d}/3$. The DUSTT code solves the equations of dust particle motion: $\mathrm{d}\boldsymbol{r}/\mathrm{d}t = \boldsymbol{v}$, $\mathrm{d}\boldsymbol{v}/\mathrm{d}t = \boldsymbol{F}_{\rm tot}/M_{\rm d} + G_{\rm col}$, together with the equations for temporal evolution of $R_{\rm d}$ and $T_{\rm d}$: $\rho_{\rm d}\mathrm{d}R_{\rm d}/\mathrm{d}t = m_{\rm d}\ (\Gamma_{\rm in} - \Gamma_{\rm out})$, and $\mathrm{d}[C_{\rm d}M_{\rm d}T_{\rm d}]/\mathrm{d}t = 4\pi R_{\rm d}^2(q_{\rm in} - q_{\rm out})$. Here operator $G_{\rm col}$ describes collisions with walls, the incident flux $\Gamma_{\rm in}$ is multi-species, the flux $\Gamma_{\rm out}$ emanating from the dust is due to reflection ($\Gamma_{\rm bsc}$) of incident particles, physical ($\Gamma_{\rm phs}$) and chemical ($\Gamma_{\rm chs}$) sputtering, radiation enhanced ($\Gamma_{\rm res}$) and thermal ($\Gamma_{\rm sub}$) sublimations. Incident heat $q_{\rm in}$ is due to ion and electron kinetic energy transfer, plasma radiation, and potential energy release, whereas the heat flux $q_{\rm out} = q_{\rm bsc} + q_{\rm rad} + q_{\rm kb}$ from dust is via reflection, thermal radiation, and kinetic and binding energy of ejected particles. We use a non-black-body expression $q_{\rm rad}(T_{\rm d}, R_{\rm d})$ generalized for arbitrary small $R_{\rm d}$. The surface potential χ is calculated by equilibrating the ion and electron fluxes at the surface: $J_{\rm e} - J_{\rm see} - J_{\rm the} = J_{\rm i}$, where $J_{\rm e}$ and $J_{\rm i}$ are the fluxes from plasma, $J_{\rm see}$ and $J_{\rm the}$ are the secondary electron and thermal electron emission fluxes. We use generalized expressions for $J_{\rm see}$ and $J_{\rm the}$ that incorporate the space charge effects. The incident fluxes: $\Gamma_{\rm in}$, $q_{\rm in}$, $J_{\rm e}$, $J_{\rm i}$, are calculated based on the OML theory. DUSTT handles the generalized case when ions and neutrals are multi-species and are in different charge states as simulated with UEDGE.

The results on dust particle dynamics are shown in Fig. 1. The calculations of two sample trajectories and corresponding evolution of dust parameters ($L_{\rm p} = \int [v_r^2 + v_z^2]^{1/2}\,\mathrm{d}t$) are done with DUSTT/UEDGE for 1-μm carbon particles launched at

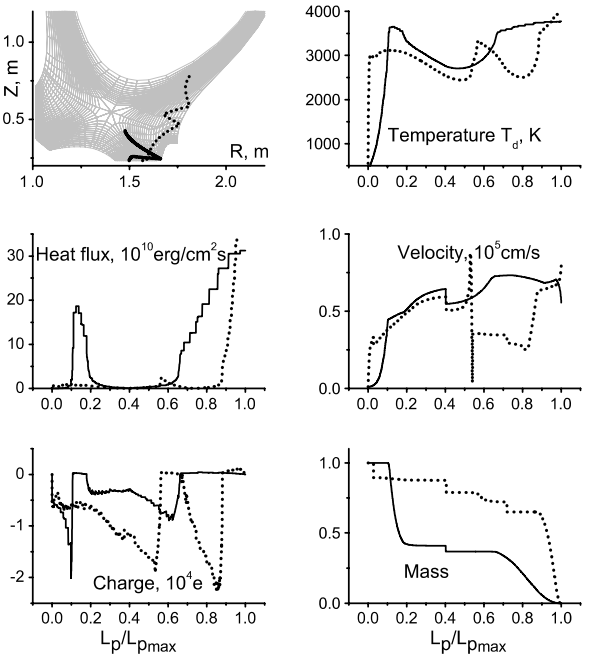

Fig. 1. Traces of 3D trajectories on UEDGE mesh for two dust particles in DIII-D discharge (upper left). Other panels display the evolution of dust parameters with the length $L_{\rm p}$.

outer divertor plate in an L-mode shot [4] on DIII-D tokamak. As seen, these dust particles are very mobile and accelerate to large velocities due to ion friction force (average speed is 400 m/s). In hot plasma regions the particles heat up to sublimation temperatures and hence efficiently lost their mass. In such regions the dust charge becomes positive due to secondary and thermal electron emissions, however, the positive charge is small because of space charge buildup. Relatively deep penetration of dust particles toward the plasma core is predicted.

3. Conditions for dust growth in plasma

Under standard plasma discharge conditions, dust particles in plasma experience the net erosion or sublimation. However, in some cases (for example, start-up and afterglow plasmas, parasitic plasmas that occur underneath a dome in some tokamaks, and highly detached divertors) the dust particles can grow from net deposition when a low-temperature, low-density plasma contains significant concentrations of intrinsic impurities.

To highlight the conditions necessary for dust growth, we use the simple model suggesting that carbon-dust particle is embedded in stationary

plasma (n_e, T_e) and neutral-gas (n_a, T_a). The deuterium plasma contains a fixed fraction γ_c of singly charged carbon ions ($[C^+] = \gamma_c n_e$) and neutrals ($[C^\circ] = \gamma_c n_a$). Input parameters are n_e, T_e, and γ_c. We assume $[D^+] + [C^+] = n_e$, $n_a = \eta_{gas} n_e$, $\eta_{gas} = 1$, $T_e = T_i$, $T_a = \eta_{ai} T_i$, $\eta_{ai} = 0.3$, and iteratively solve a set of transcendental equations involving: (1) plasma particle fluxes J_e, J_i, (2) equilibrium potential χ from $J_e - J_{see} - J_{the} = J_i$, (3) incident heat flux $q_{in}(\chi)$ and emanating radiation $q_{rad}(T_d, R_d)$, (4) equilibrium dust temperature $T_{d,eq}$ from the balance $q_{in} = q_{out}$, (5) deposition Γ_{in} and erosion Γ_{out} rates, and (6) effective erosion/deposition rate dR_d/dt from the imbalance $m_d(\Gamma_{in} - \Gamma_{out})/\rho_d$. The results of our calculations are shown in Fig. 2. The sputtering and sublimation yields depend strongly on $T_{d,eq}$. The dust temperatures in the range $700 < T_{d,eq} < 1800$ °C are favorable for deposition since chemical sputtering is suppressed while sublimation yields remain small. For 1-μm dust and $5 < T_e < 20$ eV, such $T_{d,eq}$ are attained when $0.5 < n_e/(10^{12}\ \mathrm{cm}^{-3}) < 5$. In this range of $T_{d,eq}$ and n_e, as seen in Fig. 1, even small concentrations of impurities ($\gamma_c \sim 1\%$) result in the net deposition. For $T_e = 5$ eV, $n_e = 5 \times 10^{12}\ \mathrm{cm}^{-3}$, $\gamma_c = 1\%$, we obtain $T_{d,eq} \approx 1000$ °C and dust growth rate is ~10 nm/s. In impurity rich (several %) plasmas, dR_d/dt can be ~100 nm/s. In the case of dense ($n_e > 10^{14}\ \mathrm{cm}^{-3}$, $\gamma_c \geqslant 1\%$) and cold ($T_e < 1$ eV) plasmas, dR_d/dt can attain ~1 μm/s.

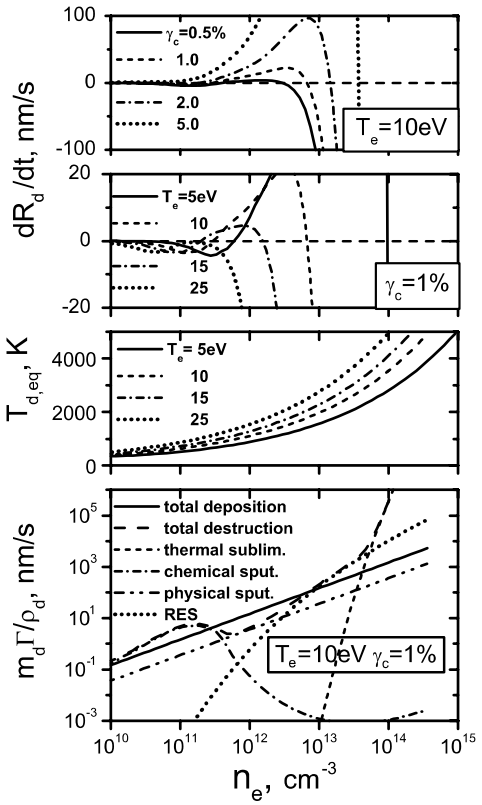

Fig. 2. Net (upper two panels) and partial (bottom) erosion/deposition rates dR_d/dt and equilibrium temperature $T_{d,eq}$ of 1-μm dust are displayed as functions of plasma density.

4. Modeling of dust spreading in a tokamak

Spreading of dust throughout the device is an important safety issue, since large amounts of dust can be mobilized in an accident (loss of vacuum [LOVA] or ingress of coolant) that may cause explosion. It is expected that dusts produced in the working chamber will penetrate far into the pumping ducts, NBI and diagnostics ports, antennae, etc. We use Monte Carlo method to evaluate the penetrability of dust particles into the rectangular ducts. We consider both horizontal and vertical (gravity directed toward the exit) ducts with dimensions $d \times d \times L$, where d and L are the width and length. We assume that incident particles have uniform distribution over the area of duct opening and over the azimuth angle and cosine of polar angle. The initial velocity v_{d0} and radius R_{d0} are input parameters. Collisions with walls are described by diffusive and mirror reflections (equal probabilities are taken here). In each collision the particle sticks to the surface with probability $1 - \gamma_m$, whereas velocity of reflected particles reduces by the factor γ_v. The real values of γ_v and γ_m are unknown. Then, we scan the γ_v and γ_m values and compute the fluxes of dust particles that stick to walls (Φ_{wal}) and leave the duct through the entrance (Φ_{rfl}) and exit (Φ_{out}) openings (the flux balance demands $\Phi_{rfl} + \Phi_{out} + \Phi_{wal} = \Phi_{in}$). The results are shown on Fig. 3 for $d = 0.1$ m, $L = 1$ m. As seen, the Φ-fluxes depend strongly on gravity, in particular, when initial velocity is small or momentum losses in wall collisions are strong. Vertical duct efficiently collects slow dust particles. The profiles of dust flux Φ penetrating into horizontal ducts are shown on Fig. 4. As seen (bottom), for strong sticking $\gamma_m \leqslant 0.5$, the penetrating flux is dominated by particles experiencing no collisions so that the dependence of Φ on γ_v is small. For high reflection probability $\gamma_m = 0.95$ (top), the highest penetration is when $\gamma_v \sim 1$. In this case, dust particles are similar to atomic particles and, asymptotically, $\Phi/\Phi_{in} \propto d/L$. Momentum losses reduce the penetration, e.g., due to gravity effects.

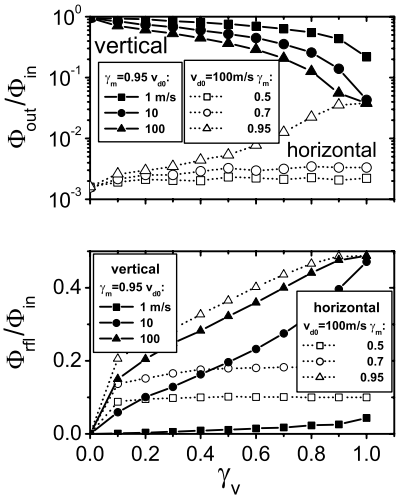

Fig. 3. Dust particle fluxes reflected from (Φ_{rfl}) and passing through (Φ_{out}) the horizontal and vertical ducts versus factor γ_v for velocity reduction in collisions.

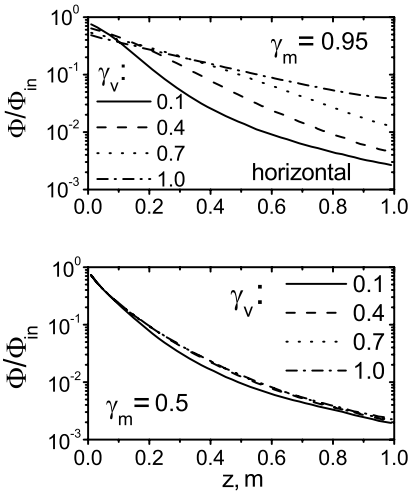

Fig. 4. Normalized flux of dust particles versus distance into the horizontal duct.

Consider conventional horizontal duct ($0.1 \times 0.1 \times 1\ m^3$) at the mid-plane of NSTX. From UEDGE modeling of typical L-mode shot we obtain the carbon ion deposition profile. Assuming that 1% of this deposit is converted into 1-μm dusts and using DUSTT we evaluate the dust flux into the duct $\Phi_{in} \approx 5 \times 10^5\ m^{-2}\ s^{-1}$, $v_{d0} = 250$ m/s, $R_{d0} = 0.85$ μm. For $\gamma_v = 0.85$, $\gamma_m = 0.6$, the flux of dust stuck to the wall at the end of the duct is $\Phi_{ac}/\Phi_{in} \approx 0.002$ and the dust mass accumulated there during experimental campaign ($\tau_c \approx 100$ days $\times 100$ shots $\times 4$ s) is 0.18 mg/m^2. The dust inventory in the duct is $\Omega_{duct} = \Phi_{wal} M_{d0} d^2 \tau_c \approx 0.8$ mg. We plan to compare simulation results with experimental data to adjust the parameters used in dust–wall interaction model.

For ITER, preliminary DUSTT/UEDGE estimates based on 0.1% conversion of plasma impurity flux into 1-μm dust particles give the dust flux $\Phi_{in} \approx 7 \times 10^6\ m^{-2}\ s^{-1}$ into a vertical duct in the private region. For a year of operation ($\tau_c \approx 3 \times 10^7$ s) the dust inventory in the duct ($0.1 \times 0.1 \times 1\ m^3$) attains $\Omega_{duct} \approx 12$ g. In LOVA accident, assuming the unity mobilization efficiency, the concentration of dust in the duct reaches $\Omega_{duct}/[d^2 L] \approx 1.2\ kg/m^3$ and substantially (20X) exceeds the lower explosion limit $\sim 50\ g/m^3$ for graphite dust in the air [5]. For complete burn up of carbon and hydrogen inventory in such explosion, we estimate that the released heat is equivalent to $W_{tnt} = 2.62\Omega_{duct} \approx 31$ g of TNT and the pressure increase is $W_{tnt}\omega_{tnt}/[3d^2 L] \approx 160$ atm, where $\omega_{tnt} = 15$ kJ/g is the heat of $C_7H_5N_3O_6$ combustion.

5. Dust profiles in tokamak plasma

We use DUSTT to calculate statistically averaged profiles of dust parameters in the tokamak plasma. Since dust generation rate and source profile are unknown, we use simplified model suggesting that (i) dust production rate is a fixed fraction ξ of total carbon erosion Ξ_{spt} by plasma, (ii) dust source profile is akin to carbon deposition profile; and (iii) angular distribution of particles is isotropic in 2π, whereas initial velocity modules is fixed. The calculations here are done under assumption that all test particles born with the same radius R_{d0} and their flux is $\Gamma_d = m_d \xi \Xi_{spt}/[4\pi\{R_{d0}\}^3 \rho_d/3]$. We take $R_{d0} = 1$ μm which is approximately the average mass-weighted radius of dust particles collected from plasma facing components after the vent-to-air in current tokamaks [4]. We use the plasma background and erosion/deposition profiles calculated with UEDGE for L-mode shot in NSTX. We launched large number ($\sim 10^5$) of test dust particles to attain satisfactory accuracy. We also assign the statistical weights to particles and employ various techniques for statistical variance reduction, e.g. suppression of dust absorption and systematic sampling of particles from sources. The calculated profile of dust particle density (all radii) is shown in Fig. 5. The dust density is peaked near the divertor plates which are the dominant dust sources. The particles quickly accelerated by plasma flow in the recycling region and spread over the divertor volumes. Due to evaporation, dust density decreases

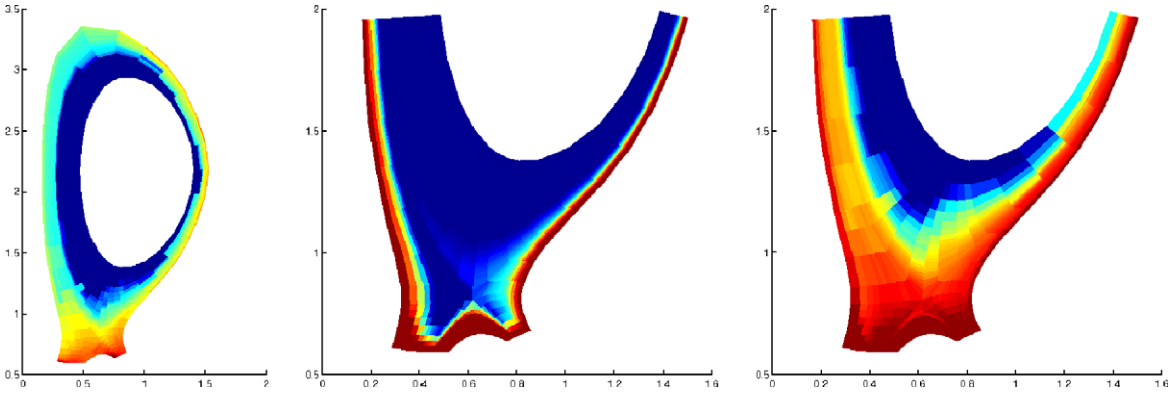

Fig. 5. Profile of dust particle density (left) calculated with DUSTT/UEDGE for NSTX. Profiles of carbon atom densities associated with usual plasma sputtering source (middle) and with 1%-deposition 1-μm dust ablation source (right). The densities increase with color changing from blue near the core to red near the walls. The middle and right panels have the same scale. (For interpretation of the references in colour in this figure legend, the reader is referred to the web version of this article.)

closer to the core. Above mid-plane the density originates predominantly from chamber wall sputtering. With DUSTT, we also calculate the source of carbon atoms due to dust ablation, and then, ablation source is inputted into UEDGE to compute the corresponding profile of neutral carbon density. The profile of carbon atoms originated from dust ablation is shown on Fig. 5 for deposit-to-dust conversion efficiency $\xi = 1\%$. It is compared to the atomic carbon density profile corresponding to the usual sputtering source. As seen, while sputtered atoms are strongly localized near material surfaces, the ablation of dust maintains relatively large impurity neutral density in the SOL and substantially enhances the impurity atom concentration in the core.

The role of dust in the impurity source advancement deep into the plasma and in the core plasma contamination is illustrated on Fig. 6. Here we compare the radial profiles of carbon atom at 7 cm below the outer mid-plane, which originate from usual sputtering source and from dust ablation sources with $\xi = 100$, 1, and 0.01%. As seen, neutral carbon density at the separatrix ($\rho = 0$) from dust ablation is comparable to that from sputtering at very low deposit-to-dust conversion efficiency: $\xi \approx 0.01\%$. In the case of $\xi = 100\%$, the carbon neutral density is even comparable to the density of deuterium neutrals around the separatrix.

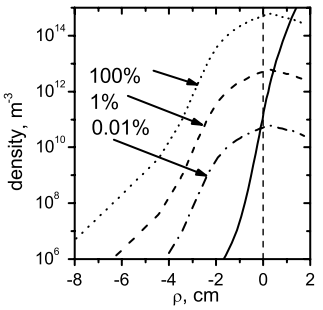

Fig. 6. Radial profiles of carbon atom density near the outer mid-plane in NSTX. The profiles are associated with sputtering impurities (solid line) and with dust ablation sources of different intensity (broken lines).

6. Discussion

Based on carbon-dust transport simulations with DUSTT and UEDGE codes, we have showed that: (1) dust particles can grow at the rate 10–100 nm/s from net deposition in the tokamak edge (isolated regions with $T_e = 5 - 10$ eV, $n_e = 10^{12}$ cm^{-3} $[C^+]/n_e > 1\%$ plasma) and up to 1 μm/s in detached plasmas; (2) if momentum loss in dust–wall collisions is small, dust particles penetrate deep into vacuum ducts, and thus, spread the hazards over a large area and increase the risk of explosion in LOVA accidents; (3) penetration of dust toward the core plasma represents a significantly enhanced impurity source there.

As follows from our UEDGE simulations (not presented here), a feedback can occur where radiation from ionized dust-related impurities can reduce the divertor temperature, which in turn allows further penetration of the dust and associated impurities. Such a feedback can result in strongly detached inner divertor-leg plasma.

In LSN configuration, the impurities sputtered from the outboard wall are entertained in the SOL

by parallel plasma flows into the inner divertor and are deposited on the plate. Experiments showed that the inner plate (IP) exhibits net deposition. According to UEDGE modeling, the amount of material carried by plasma flow (about several amperes in L-mode shots) is approximately equal to net deposition rate. Along with impurities, the IP is expected to retain more working gas (tritium in ITER). At the same time, dust particles originating from IP preferentially move outboard due to centrifugal force resulting from dust acceleration by toroidal plasma flows. Hence, dust can potentially connect the material migration in a loop. To study material migration loop, we intend to perform fully self-consistent modeling of plasma, impurities, and dust transport with coupled DUSTT and UEDGE codes.

It is important to note that there is a lack of experimental data on thermo-chemical properties and shape of dust particles, dust production rates are unknown, and there are uncertainties in the dust–plasma and dust–wall interactions. Hence, much more studies in dust-related areas are required. Routine experiments on 3D measurements of incandescent dust particle trajectories are planed on several tokamaks (e.g. on NSTX [6]) and we will use this data for validation and verification of the DUSTT code.

References

[1] G.F. Federici et al., Nucl. Fusion 41 (2002) 1967.
[2] C. Gordon et al., Fusion Eng. Des. 55 (2001) 347.
[3] S.I. Krasheninnikov et al., Phys. Plasmas 11 (2004) 3141.
[4] A.Yu. Pigarov et al., Phys. Plasmas 12 (2005) 122508.
[5] P. van der Wel et al., Part. Part. Syst. Charact. 8 (1991) 90.
[6] A.L. Roquemore et al., J. Nucl. Mater., these Proceedings, doi:10.1016/j.jnucmat.2007.01.065.